Climate variability – observations, reconstructions, and model simulations for the Atlantic-European and Alpine region from 1500–2100 AD

**Christoph C. Raible · Carlo Casty · Jürg Luterbacher ·
Andreas Pauling · Jan Esper · David C. Frank ·
Ulf Büntgen · Andreas C. Roesch · Peter Tschuck ·
Martin Wild · Pier-Luigi Vidale · Christoph Schär ·
Heinz Wanner**

Abstract A detailed analysis is undertaken of the Atlantic-European climate using data from 500-year-long proxy-based climate reconstructions, a long climate simulation with perpetual 1990 forcing, as well as two global and one regional climate change scenarios. The observed and simulated interannual variability and teleconnectivity are compared and interpreted in order to improve the understanding of natural climate variability on interannual to decadal time scales for the late Holocene. The focus is set on the Atlantic-European and Alpine regions during the winter and summer seasons, using temperature, precipitation, and 500 hPa geopotential height fields. The climate reconstruction shows pronounced interdecadal variations that appear to "lock" the atmospheric circulation in quasi-steady long-term patterns over multi-decadal periods controlling at least part of the temperature and precipitation variability. Different circulation patterns are persistent over several decades for the period 1500 to 1900. The 500-year-long simulation with perpetual 1990 forcing shows some substantial differences, with a more unsteady teleconnectivity behaviour. Two global scenario simulations indicate a transition towards more stable teleconnectivity for the next 100 years. Time series of reconstructed and simulated temperature and precipitation over the Alpine region show comparatively small changes in interannual variability within the time frame considered, with the exception of the summer season, where a substantial increase in interannual variability is simulated by regional climate models.

C. C. Raible
Climate and Environmental Physics, Physics Institute, University of Bern, Sidlerstrasse 5, CH-3012
Bern, Switzerland

C. Casty · J. Luterbacher · A. Pauling · H. Wanner
Institute of Geography, University of Bern, Hallerstrasse 12, CH-3012 Bern, Switzerland

J. Esper · D. C. Frank · U. Büntgen
Swiss Federal Research Institute WSL, Zürcherstrasse 111, CH-8903 Birmensdorf, Switzerland

A. C. Roesch · P. Tschuck · M. Wild · P.-L. Vidale · C. Schär
Institute for Atmospheric and Climate Science ETH, Winterthurerstrasse 190, CH-8057 Zürich,
Switzerland

1 Introduction

Observations and reconstructions for the late Holocene show that the warming since the 1960s is likely unprecedented over the last millennium (Jones and Mann 2004). Modelling studies give some evidence that the temperature change of at least the second half of the 20th century can only be explained by including anthropogenic forcing (Rind et al. 1999; Crowley 2000; IPCC 2001; Meehl et al. 2003; Bauer et al. 2003). Nevertheless, to assess future climate change for key regions, like the Atlantic-European area, with confidence, a thorough understanding of the underlying mechanisms of natural climate variability on different spatio-temporal scales for the late Holocene is necessary (Jones and Mann 2004).

One possibility to address the understanding of natural climate variability of the Atlantic-European region is to investigate general circulation models (GCMs). Modelling results show that for the mid-latitudes the coupling between atmosphere and ocean plays a major role on decadal variability (Grötzner et al. 1998; Raible et al. 2001; Marshall et al. 2001, and references therein). This coupling has implications for the low-frequency (decadal) behaviour of the North Atlantic Oscillation (NAO), with its well-known linkage to temperature and precipitation on the interannual time scale (Hurrell 1995; Hurrell and Loon 1997; Wanner et al. 2001; Hurrell et al. 2003). Even baroclinic high-frequency variations characterised by stationary and transient wave activity should be incorporated to understand enhanced low-frequency variability of the NAO (Raible et al. 2004). Additionally, future projections integrated with coupled atmosphere-ocean (AO-) GCMs show a systematic northeastward shift of the northern center of action of the NAO (Ulbrich and Christoph 1999), indicating that at least the modelled position of the pressure centers is not stable in time. Recently, a strong connection between sea surface temperature (SST) and the North Atlantic Thermohaline Circulation has been presented in unforced control AO-GCM simulations (Latif et al. 2004; Cheng et al. 2004). These SST anomalies, containing strong multi-decadal variability, may mask anthropogenic signals in the North Atlantic region. Another potential mechanism of generating low-frequency NAO variability is the stratosphere, where stratospheric processes can be influenced by changes in the external solar and volcanic forcing (Shindell et al. 2001, 2003). Another problem present in this region is illustrated by an ensemble modelling study for the Maunder Minimum from 1640 to 1715 (Yoshimori et al. 2005), showing that forcing signals, e.g., solar forcing, are difficult to detect due to the strong internal variability induced by the NAO.

Another approach to improve our understanding of natural climate variability is to extend the existing climate records for temperature, precipitation, and atmospheric circulation patterns back in time. One first step was to reconstruct temperature on hemispheric to global scales over the past centuries to millennia based on empirical proxy data (Bradley and Jones 1993; Overpeck et al. 1997; Jones et al. 1998; Mann et al. 1998; Briffa et al. 2001; Esper et al. 2002a; Cook et al. 2004; Jones and Mann 2004; Esper et al. 2004; Moberg et al. 2005). However, hemispheric-scale reconstructions provide little information about regional scale climate variability. Therefore, studies focusing on reconstruction of specific regions, e.g., Atlantic-Europe or high Asia, utilising documentary (Luterbacher et al. 2004; Xoplaki et al. 2005; Guiot et al. 2005) and tree-ring data (Esper 2000; Esper et al. 2002b, 2003; Büntgen et al. 2005) are also valuable.

Jones et al. (2003) found amongst others changes in the annual cycle of Northern Hemisphere temperatures indicating that, compared with earlier times, winters have warmed more relative to summers over the past 200 years.

A third research focus is on atmospheric circulation variability. Besides traditional reconstructions of the NAO index (Appenzeller et al. 1998; Luterbacher et al. 2002a; Cook

et al. 2002; Vinther et al. 2003), atmospheric circulation modes (Jacobeit et al. 2003) for each month in the year were derived from sea-level pressure field reconstructions (Luterbacher et al. 1999, 2002b). Utilising reconstructions of the 500 hPa geopotential height fields for the Atlantic-European region, Casty et al. (2005a) found that climate regimes, defined by the joint probability density function of the first two leading Empirical Orthogonal Functions, are not stable in time.

With a steadily growing data base, it is now possible to reconstruct climate variations from small regions like the European Alps (Casty et al. 2005b; Frank and Esper 2005; Büntgen et al. 2005). This could help to place extreme events, e.g., the hot European summer of 2003 (with its maximum deviation from the mean in central Europe and the Alps), in a longer-term context (Luterbacher et al. 2004). Recently, regional modelling studies (Schär et al. 2004) showed that in a scenario with increased atmospheric greenhouse-gas concentrations, future European temperature variability may increase by up to 100%, with maximum changes in central and eastern Europe. Such a change in variability would have a strong impact on not only the environment, but also on the society and the economy in these regions.

The National Center of Competence in Research on Climate (NCCR Climate) in Switzerland provides a substantial variety of different spatio-temporal highly-resolved climate information, ranging from natural and documentary proxy reconstructions, to high-quality instrumental measurements, to modeled data from state-of-the-art general circulation and regional models for both present day climate conditions (fixed to 1990 AD) as well as future scenarios. The aim of this study is to combine the two major types of information in the archive – the observations and reconstructions on the one hand, and the simulations for present day climate conditions and future scenarios on the other hand. This set of data and simulations will form the basis for the investigation of the atmospheric circulation and its links to the behaviour of temperature and precipitation in the Atlantic-European and the Alpine regions on interannual to decadal time scales. Additionally, changes in the annual cycle from 1500–2100 AD are discussed.

The outline of this paper is as follows: In Section 2 the reconstructed and modeled data, as well as some analysis techniques and definitions, are introduced. Subsequent analysis concentrates on the Atlantic-European (Section 3) and Alpine (Section 4) regions, illustrating the relationship between large-scale flow regimes and temperature and precipitation. The results are summarised and interpreted, in the context of published evidence, in Section 5.

2 Reconstructions, models, and analysis techniques

The study is based on a set of reconstructed and modeled data, which is introduced as follows. We focus on winter (December to February, DJF) and summer (June to August, JJA) of the Atlantic-European and the Alpine regions, respectively.

2.1 Reconstructions and models

Reconstructions of past pressure, temperature, and precipitation are performed through multivariate statistical climate fields reconstruction (CFR) approaches. CFR seeks to reconstruct a large-scale field by regressing a spatial network of proxy indicators (e.g., early instrumental, tree-ring data, and historical evidences) against instrumental field information (Jones and Mann 2004). During periods when both proxy and instrumental field information (reanalyses) are available, regression models are developed and fed with proxy data to reconstruct past climate variables.

For the Atlantic-European region reconstructions of seasonally resolved land surface air temperature (Luterbacher et al. 2004, 25°W–40°E and 35°N–70°N), precipitation (Pauling et al. 2006, 10°W–40°E and 35°N–70°N), and 500 hPa geopotential height fields (Luterbacher et al. 2002b, 30°W–40°E and 30°N–70°N) are available back to 1500. Independent reconstructions, i.e., sharing no common predictors, have been developed for seasonal land surface air temperatures and precipitation fields for the European Alps since 1500 (Casty et al. 2005b, 4°E–16°E and 43°N–48°N). These CFRs are multi-proxy based. The period from 1500 to the late 17th century comprises entirely documentary and natural proxies; the period from 1659 to around 1750 includes a mix of documentary, natural proxies as well as a few early instrumental data. The reconstructions for the last 250 years are entirely based on instrumental time series, the number of those increasing steadily over time. A compilation of all proxies and instrumental data used for those 500 year climate reconstructions is given in Luterbacher et al. (2004), Casty et al. (2005b), and Pauling et al. (2006). The spatial resolution for the temperature and precipitation reconstructions is 0.5° (∼60 km × 60 km) similar to the instrumental field information for the 1901–2000 period: Instrumental data from New et al. (2000) were used by Luterbacher et al. (2004); data from Mitchell et al. (2004) were used by Casty et al. (2005b) and Pauling et al. (2006). The 500 hPa fields are resolved on a 2.5° grid similar to the NCEP Reanalysis data (Kalnay et al. 1996; Kistler et al. 2001). For further details about reconstruction methods, proxy information, verification, and uncertainty estimates, the reader is referred to Luterbacher et al. (2002b, 2004), Casty et al. (2005b), and Pauling et al. (2006).

A new millennial-long tree-ring reconstruction utilising 1527 ring width measurement series from living and relict larch and pine samples from the Swiss and Austrian Alps (46.5°N–47°N and 7.5°N–11.5°E) is applied for further comparison and validation (Büntgen et al. 2005). This record was detrended using the Regional Curve Standardisation (RCS) method (Briffa et al. 1992), and calibrated and verified against high elevation station temperature data (Böhm et al. 2001) over the 1864–2002 period. Note that this reconstruction is independent from Casty et al. (2005b).

Two different ocean-atmosphere general circulation models (OA-GCMs) are used in this study. The first model is the Max Planck Institute for Meteorology global coupled model, ECHAM5/MPI-OM. The resolution of the atmospheric component, ECHAM5 (Roeckner et al. 2003, version 5.0), is 19 levels in the vertical dimension and T42 in spectral space, which corresponds to a horizontal resolution of about 2.8° × 2.8°. The oceanic component, MPI-OM (Marsland et al. 2003), is based on a Arakawa C-grid (Arakawa and Lamb 1981) version of the HOPE ocean model (Wolff et al. 1997). It is run on a curvilinear grid with equatorial refinement and includes 20 vertical levels. A dynamic/thermodynamic sea ice model (Marsland et al. 2003) and a hydrological discharge model (Hagemann and Duemenil-Gates 2001) are included. The atmospheric and oceanic components are connected with the OASIS coupler (Terray et al. 1998). The model does not employ flux adjustment or any other corrections. Initial ocean conditions are taken from a 500-yr control integration. The model is forced from stable conditions with a 1% CO_2 increase per year from 1990 (348 ppm) to 2100 (1039 ppm). Hereafter, this experiment is denoted as ECHAM5 1% CO_2. This forcing is a commonly used scenario to intercompare the sensitivity of different coupled climate models to increased greenhouse gases.

The second setup is the Climate Community System Model (CCSM), version 2.0.1,[1] developed by the National Center for Atmospheric Research (NCAR) (Kiehl et al. 1998;

---

[1] http://www.ccsm.ucar.edu/models/

Blackmon et al. 2001). The atmospheric part of this coupled model has a horizontal resolution of T31 (∼3.75° × 3.75°) with 26 vertical levels; the ocean component has ∼3.6° × 1.8° resolution with 25 levels. The CCSM also runs without any flux corrections. Two simulations were carried out: a 550-yr simulation for constant present day climate conditions fixed to 1990 AD (denoted as CCSM 1990) and a 1% CO_2 simulation (denoted as CCSM 1% CO_2) starting from the stable state of the CCSM 1990 (Raible et al. 2005). Note that for the CCSM 1990, the first 50 years are ignored until the model adjusts to its stable climate state. The CCSM is integrated on two different computer platforms, an IBM SP4 and a Linux cluster (Renold et al. 2004). Note that the different computer platforms have no influence on the mean behaviour of the simulations.

Regionally, we use the Climate High Resolution Model (CHRM) which is driven by the Hadley Center HadAM3 atmospheric GCM at the lateral boundary (Pope et al. 2000). The CHRM regional model covers Europe and a fraction of the North Atlantic on a 81 by 91 grid point domain with a resolution of approximately 56 km and a time step of 300 s (see Vidale et al., 2003 for model set-up). The CHRM has been validated regarding its ability to represent natural interannual variations (Vidale et al. 2003) and the precipitation distribution in the Alpine region (Frei et al. 2003) using a simulation that is driven by the ECMWF reanalysis ERA-15 (Gibson et al. 1999). Two time-slice simulations are performed: For the control simulation from 1961–1990 the HadAM3 and the nested CHRM uses observed SSTs and observed greenhouse gas concentrations. The second experiment for the time-slice 2071–2100 uses the forcing of an IPCC A2 scenario (IPCC 2001). To assure that changes in variability between the two simulations are not associated to SST changes, but are due to the atmospheric models and their interaction with the land surface, the so-called delta change approach is applied to the experimental setup (Jones et al. 2001). Both GCM HadAM3 simulations, delivering the boundary conditions for the CHRM regional model, use the same SST variations (taken from the 1960–1990 observations), but a mean SST warming is added to the A2 scenario simulations by using the warming signal from the coupled HadCM simulation. Both simulations have a one year spin-up phase: 1960 and 2070, respectively.

2.2 Analysis techniques

The analysis presented in this paper is restricted to the Atlantic-European and the Alpine region. Time series are defined for both regions. The temperature time series is the mean over 25°W–40°E and 35°N–70°N for the European land area and over 4–16°E and 43–48°N for the Alpine region. For the precipitation time series the Atlantic-European region was reduced to 10°W–30°E and 35°N–70°N due to the smaller area available from the reconstructions (Pauling et al. 2006). To emphasise and extract low-frequency variability, a 31-yr triangular filter was applied. The first and the last 15 years of the time series are not analysed to avoid edge effect problems.

To merge the time series from climate simulations and reconstructions, and to account for biases of the model simulations, anomalies with respect to the overlapping 1990–2000 and 1961–1990 periods were used for the Atlantic-European and the Alpine area, respectively. Biases between the model output and the reconstructions are amongst others due to the coarse model resolution (horizontally and vertically) and the inclusion of sea areas which are not considered in the reconstructions. Moreover, due to the different horizontal resolution the size of the area slightly varies from the reconstructions. Other reasons for biases could also be the uncertainties of the proxy input data of the reconstruction method as well as systematic model errors, e.g., model drifts and underestimation of subgrid scale variability. Filtering
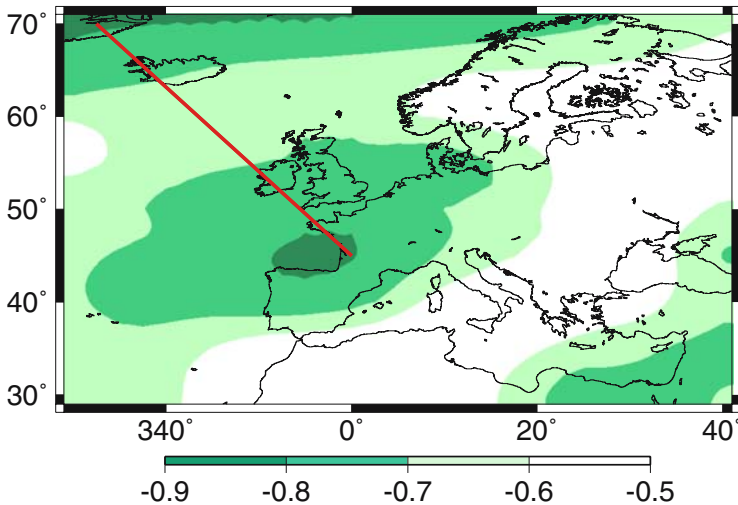
Fig. 1 An example of a 30-yr window (1973–2002), where the teleconnectivity of the 500 hPa geopotential height (DJF, shaded) and the corresponding axis of teleconnectivity (red line) is denoted

was applied to each time series separately in order to avoid mixing model and reconstruction data. However, this results in gaps in the filtered time series.

The spatio-temporal behaviour of the circulation of the free atmosphere can be characterised by the teleconnectivity of the 500 hPa geopotential height. According to Wallace and Gutzler (1981) the teleconnectivity is defined as the strongest negative correlation of one base point with all grid points assigned at the base point. As base point, all grid points are iteratively chosen. Only strong negative correlations which cluster together in a large area are considered as "centers of action". Thus, anticorrelated centers of action, e.g., the NAO with its poles near Iceland and the Azores, are easily identified. To find the center that is anticorrelated with another one, a search algorithm is applied to the teleconnectivity map. In a $20° \times 10°$ longitude/latitude neighbourhood the strongest negative correlation coefficient is identified. Provided that the region is large enough to capture one center of action, the size of search area is not a critical factor in this procedure. Then, this grid point is again correlated with all others in the 500 hPa geopotential height providing the position of the grid point which has the strongest negative correlation. These positions are connected with lines denoting the axis of the opposing centers of action. In order to illustrate this method, Figure 1 shows the teleconnectivity of the reconstructed 500 hPa geopotential height (shadings) in winter (DJF) and the axis of the anticorrelated centers of action (red line) for the 1973 to 2002 period. The two centers of action are easily identified. Perpendicular to the axis, the atmospheric flow is strengthened or weakened, depending on the sign of the centers of action. For example, if the northern center is negative and the southern is positive, the westerly atmospheric flow is stronger than average, and vice versa.

The technique was applied to the 500 hPa geopotential height data for a 30-yr running window, where only the axes of the conversing centers of action are displayed. This results in a three-dimensional Hovmöller diagram (e.g., Figure 5) which shows the spatio-temporal behaviour of atmospheric circulation patterns. The window size was chosen to fit to the filter applied to the time series and also to correspond to the window regularly used for time-slice experiments with highly resolved climate models in the climate change community (Wild

et al. 2003). Another reason for setting the size to 30 years is that the World Meteorological Organisation defines climatological mean to be a 30-yr mean. Nevertheless, tests with moderate changes of the window size, e.g., 40 years, confirm the results in the following sections.

3 Climate variability in the Atlantic-European area

To investigate climate variability in the Atlantic-European region we first focus on the reconstructed time series. The interannual variation of the temperature reconstruction (Luterbacher et al. 2004, Figure 2a,b) shows larger variability in winter (standard deviation of 1.1 °C) than in summer (standard deviation of 0.44 °C). This is in contrast to the three simulations, showing a standard deviation of about 0.65 °C in winter and 0.4 °C in summer, and illustrating a model deficiency in winter and/or the difference calculating the averages for different resolution. Comparing the CCSM 1990 simulation with the two scenario simulations, the variability on this time scale is nearly equal. Note that other simulations, especially regional simulations, show this variability change from winter to summer and therefore a better agreement with the observations and the reconstructions (IPCC 2001).

The reconstructed and simulated precipitation time series (Pauling et al. 2006, Figure 2c,d) show a slightly smaller interannual variability than in the observed period 1900–2000. Before 1800 the variability of the seasonally reconstructed precipitation (Figure 2c) decreases. For the first 300 years only a few natural proxies in combination with documentary precipitation information, unevenly distributed over Europe, are available. These scattered data obviously cannot fully resolve the variance at continental scale, thus the statistical method tends to calibrate more towards the long-term 20th century mean (climatology), and due
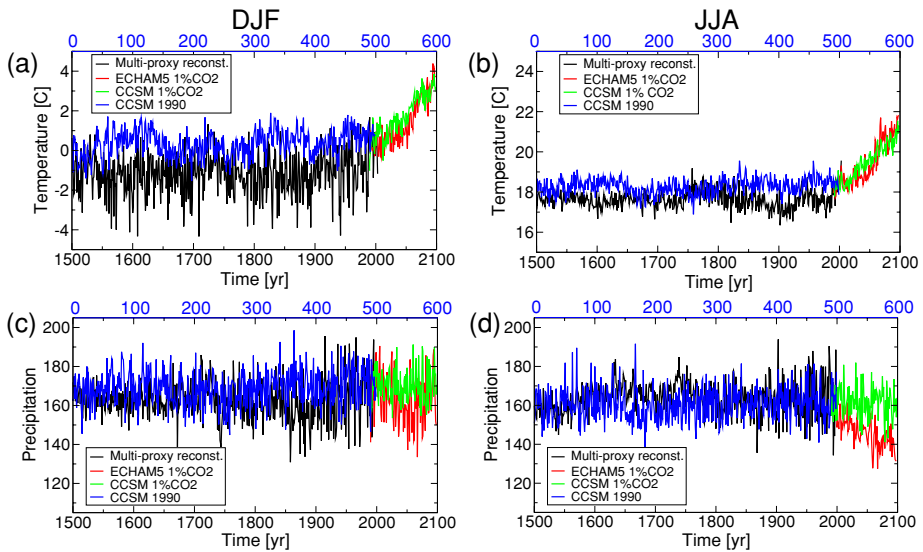

Fig. 2 Unfiltered time series of European temperature and precipitation for (a,c) DJF and (b,d) JJA. The time series are adjusted to the period 1990-2000. The multi-proxy reconstructions are based on Luterbacher et al. (2004) for temperature and Pauling et al. (2006) for precipitation (unit: mm per 3 months). Note also that the CCSM 1990 simulation is for perpetual 1990 conditions, thus the top blue *x*-axis shows model years

to the low number of degrees of freedom "extremes" are not well reconstructed. Over the last 200 years, when widespread instrumental precipitation data become available, the uncertainties in terms of unresolved variance within the 20th century calibration period, decrease and more accurate reconstructions are obtained. The interannual variability is further reduced in the scenario simulations (ECHAM5 and CCSM 1%CO_2) compared with the CCSM 1990 particularly in summer despite the fact that each model has its own climate sensitivity.

Switching to low-frequency variability, emphasised by a 31-yr triangular filter, the temperature reconstructions show several distinct cold phases, namely during the late 16th, late 17th and late 19th centuries (Figure 3a). Interestingly, the cold winter conditions during the last decades of the 17th century correspond to a period of low solar activity known as the Maunder Minimum. Comparing the CCSM 1990 with the reconstructed temperature, the low-frequency variability diverges, showing colder temperatures for the reconstructions in both seasons. This is not surprising since the radiative forcing of the simulation is set to fixed 1990 conditions (solar and greenhouse gas concentrations), whereas the observed mean radiative forcing over the past 500 years is lower than the 1990 value. However, the range of decadal variations is similar for the CCSM 1990 and the reconstruction from 1500–1900 leading to a signal detection problem as mentioned by Yoshimori et al. (2005). They showed in a modelling study of the Maunder Minimum that temperature variation on a hemispheric scale could be partly traced back to changes in the external forcing. On a regional scale this is more difficult, particularly in areas where the internal variability is high, e.g., the exit regions of the midlatitude storm tracks (Alaska, Atlantic-European area). As expected, the scenario simulations show for both seasons a strong temperature increase towards 2100. This increase
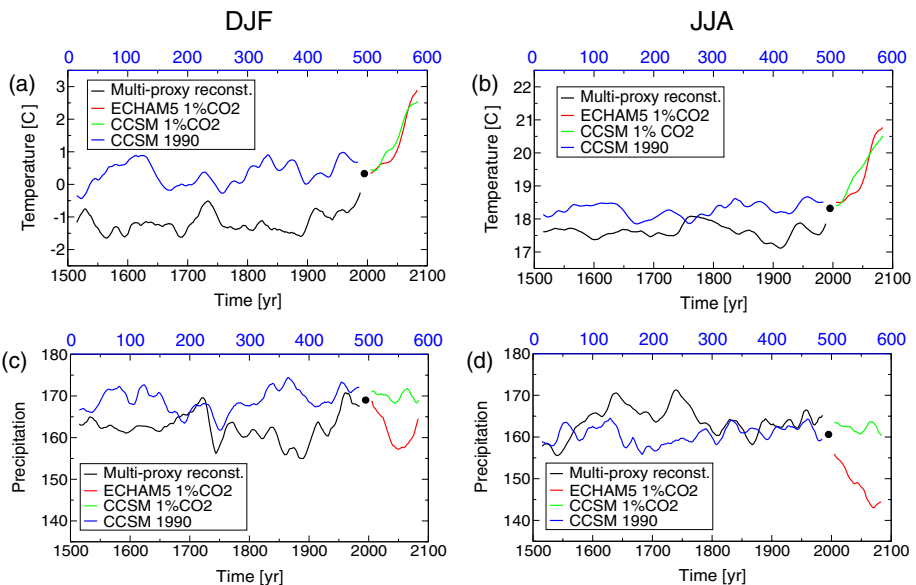

Fig. 3 Filtered time series of European temperature and precipitation for (a,c) DJF, (b,d) JJA. The time series are adjusted to the period 1990–2000 (denoted by the black dot). A 31-yr triangular filter is used emphasising the low-frequency variability in the time series. The multi-proxy reconstructions are based on Luterbacher et al. (2004) for temperature and Pauling et al. (2006) for precipitation (unit: mm per 3 months). Note also that the CCSM 1990 simulation is for perpetual 1990 conditions, thus the top blue x-axis shows model years

is unprecedented compared with increases in the CCSM 1990 or the reconstruction prior to 1900.

The low-frequency behaviour of precipitation (Figure 3c,d) also shows remarkable variations in the last centuries, but is reduced in the CCSM 1990 simulation compared with the reconstruction. The standard deviation of the filtered time series is reduced from 3.4 to 2.7 mm per three months in winter and from 3.5 to 2.1 mm per three months in summer, respectively. The scenario simulations show a decrease of precipitation mainly in summer.

To investigate seasonality in more detail, the difference between JJA and DJF is compared for temperature and precipitation (Figure 4) as suggested by Jones et al. (2003). However, a part of this difference may be due to the lack of variability in volcanic and solar forcing in the simulation (Hansen et al. 1992). Clearly the range of variation of the temperature difference (Figure 4a) is stronger in the reconstructions than in the model simulations resembling the results of Jones et al. (2003). Moreover, a negative trend from the 19th century to the 20th century is evident in the reconstructions. This decrease of summer to winter temperatures may also continue in the future as the CCSM 1% CO_2 in comparison to the CCSM 1990 suggests. Again, one has to be cautious as the other scenario does not show such a decrease.

For the precipitation difference, the range of variation is again stronger in the reconstructions than in the model simulations (Figure 4b). One scenario simulation (ECHAM5 1% CO_2) shows a decrease in precipitation seasonality. Notable is an increased seasonality in precipitation after the Late Maunder Minimum (∼1720) which goes along with a strong decrease of temperature difference. However, due to increased uncertainties prior to the 18th century the seasonality changes of the reconstruction have to be interpreted with caution.

The low-frequency changes of temperature and precipitation as well as their changes in seasonality may be related to low-frequency changes of the atmospheric flow-regime. Therefore, the temporal teleconnection behaviour illustrated by the teleconnectivity of the 500 hPa geopotential height is shown for the reconstructions (Luterbacher et al. 2002b; Casty et al. 2005a, Figure 5). In winter two direction axes are frequently revisited (Figure 5a, bottom panel): a north-south axis, denoting an anomalous (stronger or weaker) westerly flow towards Europe, and a northwest-southeast axis exhibiting an anomalous meridional flow towards Europe. Temporally these patterns are stable for several decades (Figure 5a, top panel). The 16th century indicated by (i) is dominated by the anomalous meridional flow pattern, switching to the westerly pattern from ∼1600 to 1650 (ii in Figure 5a, top panel). Note that this westerly pattern is mainly in its negative phase, so continuing an anomalous meridional flow. For the Late Maunder Minimum period (∼1680 to 1715, iii) the axis turns again towards the northwest-southeast orientation and the position of the northwestern center moves from Iceland to the British Islands. For the 20th century the axis shows again a north-south orientation.

During summer a different picture with a northwest-southeast and a southwest-northeast orientation of the axis of teleconnectivity is captured (Figure 5b, bottom panel). A west-east orientation can also be found, but this is a rare event and therefore not of primary consideration. For the northwest-southeast orientation, main air masses stem from western Russia (positive phase) or the southern Atlantic (negative phase). The southwest-northeast corresponds to a flow regime from Greenland (positive phase) or North Africa (negative phase). Temporally the southwest-northeast orientation, corresponding to an anomalous stronger or weaker north-south flow, was mainly found in the 17th century, which was dominated by the Maunder Minimum (Figure 5b, top panel). From 1720 onwards the climate system stays in the northwest-southeast mode. The anticorrelations are less pronounced in summer compared to winter (not shown).
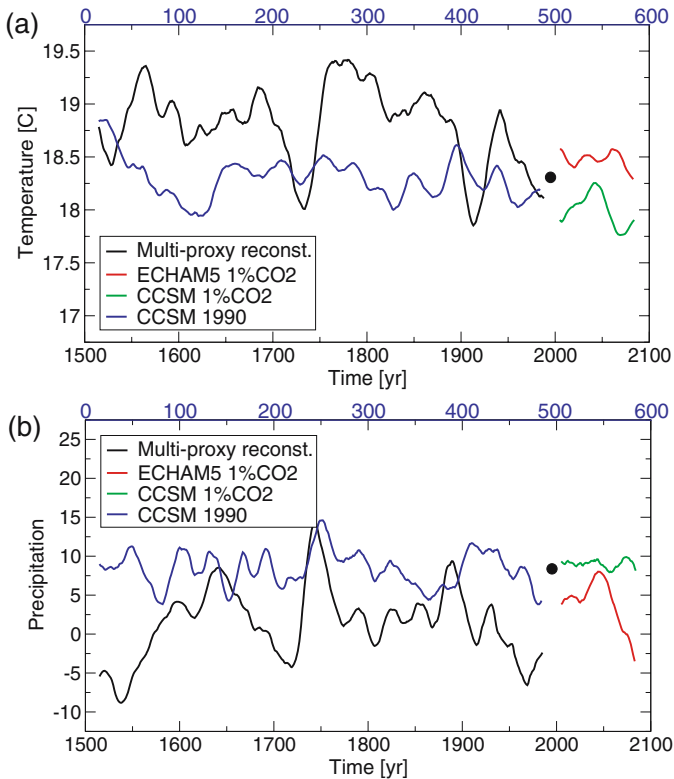
Fig. 4 Filtered time series for the difference JJA-DJF (a) European temperature and (b) European precipitation (unit: mm per 3 months). The time series are adjusted to the period 1990–2000 (denoted by the black dot). A 31-yr triangular filter is used emphasising the low-frequency variability in the time series. The multi-proxy reconstructions are based on Luterbacher et al. (2004) and Pauling et al. (2006). Note also that the CCSM 1990 simulation is for perpetual 1990 conditions, thus the top blue x-axis shows model years

The orientations of the teleconnectivity in the CCSM 1990 simulation behave differently. The CCSM 1990 shows a northwest-southeast axis and a north-south axis (Iceland to Azores) in winter, which is similar to the reconstructions, but there is also a north-south anticorrelation from Scandinavia to the eastern part of the Mediterranean Sea (Figure 6a). Temporally, the axis orientation is not stable in time for decades which is also in contrast to the reconstructions. The summer (Figure 6b) behaves temporally similar to winter, but also exhibits the southwest-northeast axis found in the reconstructions. Overall the simulated teleconnection evolution appears more noisy and less structured than the reconstruction teleconnections (Figure 5) for both seasons.

In contrast to the CCSM 1990 simulation, the teleconnection patterns in the scenario simulations are more time stable over several decades for both seasons (Figure 7). The ECHMA5 1% CO_2 resembles the reconstruction modes, whereas in the CCSM 1% CO_2 the position of the northwestern center of the northwest-to-southeast mode in winter is moved to Britain Isles. In summer the southeast center of the CCSM 1% CO_2 simulation is moved to the Iberian peninsula, in contrast to the reconstructions and the other simulations where this center of action is located in the eastern part of the Mediterranean Sea. Whether or not
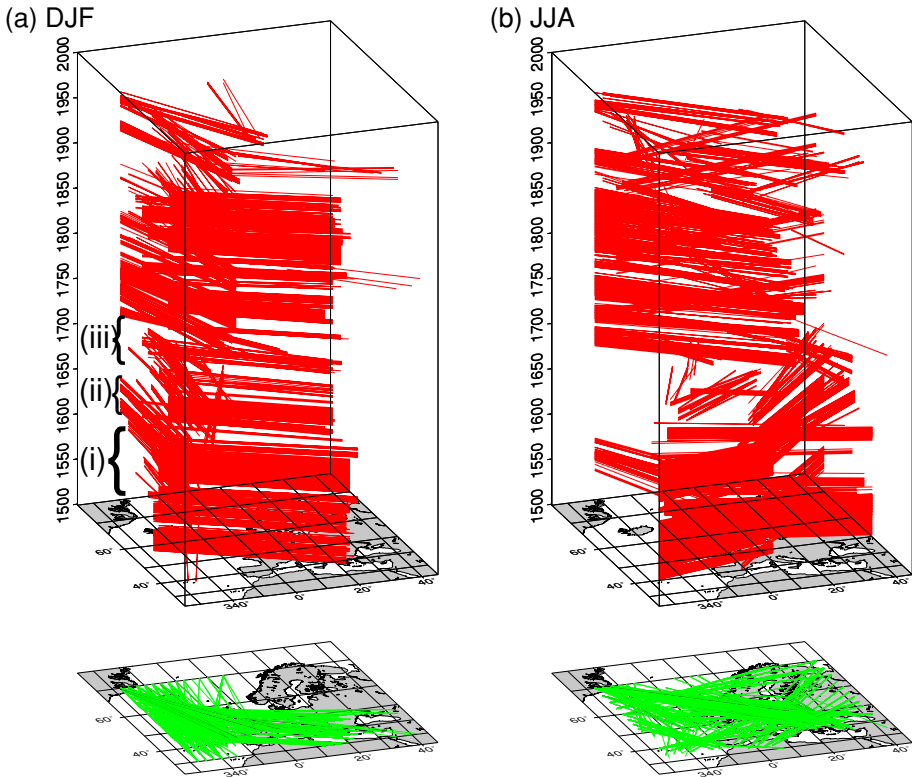
Fig. 5 The temporal evolution of the axis of teleconnections measured by the teleconnectivity of the reconstructed 500 hPa geopotential height (Luterbacher et al. 2002b): (a) DJF and (b) JJA. Bottom panels show the projection of all axes in the Atlantic-European region. The axes connect the centers of action within particular teleconnection modes. Special periods mentioned in the text are indicated by (i), (ii), and (iii)

this is a model deficiency or a real signal to the 1% CO_2 increase can not yet be concluded. Ensemble simulations with more than two models, in order to minimise the influence of specific model formulations, could help answer this question.

Combining the results of Figure 2 through Figure 7, we find for the cold spell during the 17th century, corresponding to the Maunder Minimum that winters were colder and drier, and summers were colder and wetter than today (Luterbacher et al. 2001). An abrupt seasonality change in temperature and precipitation occurred at or near the end of the Maunder Minimum. In both seasons the atmospheric circulation changed to a more meridional mode during the Maunder Minimum where the axis, connecting the centers of action, exhibits a northwest-southeast orientation in winter and a southwest-northeast orientation in summer. Nevertheless, one has to mention that the Maunder Minimum is not the only cold period; also the end of the 16th and 19th centuries colder seasons compared to today are observed with similar shifts of teleconnection patterns. Moreover, the teleconnection patterns are more time stable in the reconstruction. A more variable temporal behaviour of the simulated teleconnectivity of CCSM 1990 is observed and could be due to model deficiencies and/or the constant external forcing compared with the reconstructions. The reconstruction method itself could also be the source of generating stability over several decades by focusing on only a few
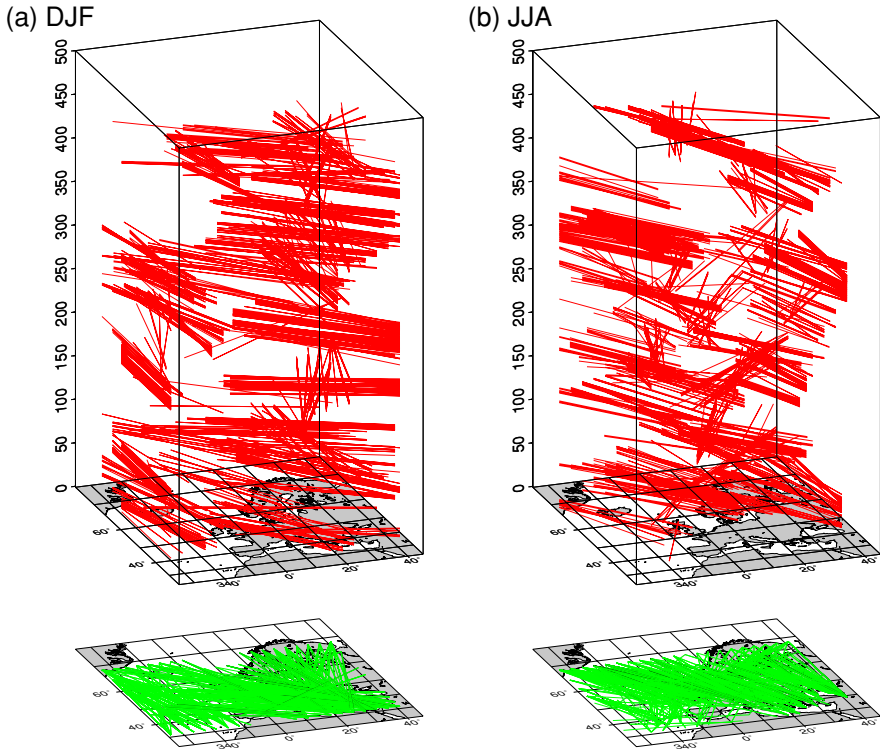
(a) DJF   (b) JJA

Fig. 6 Same as Figure 5, but for the 500-year long CCSM simulation with perpetual 1990 conditions

patterns of variability. But, because the reconstructions incorporate external forcing ranging from natural (solar and volcanic) to anthropogenic forcing (greenhouse gas emissions) and because the scenario simulations show a greater time stability of the teleconnection pattern (compared with the CCSM 1990) we favor an influence of external forcing, thus we hypothesise that time-dependent external forcing (solar, volcanic and greenhouse gases) might help in stabilising the mode temporally.

4 Climate variability in the Alps

With the steadily growing data base, reconstructions of climate parameters are performed for the European Alps (Casty et al. 2005b; Frank and Esper 2005; Büntgen et al. 2005). Figures 8 and 9 show the winter (DJF) and summer (JJA) temperature and precipitation for the Alpine areas, respectively. In winter, the temperature shows periods with stronger interannual variations around 1600 and a decrease in this variability in the second half of the 20th century (Figure 8a). In summer, where two independent reconstructions are available, the interannual variations are nearly unchanged, except for the period 1800–1830 which was dominated by strong volcanic eruptions, e.g., 1815 eruption of Tambora (Figure 8b). Comparing both reconstructions, stronger variability is found within the multi-proxy reconstruction (Casty et al. 2005b). This is likely due to the fact that although the tree-ring reconstruction has a
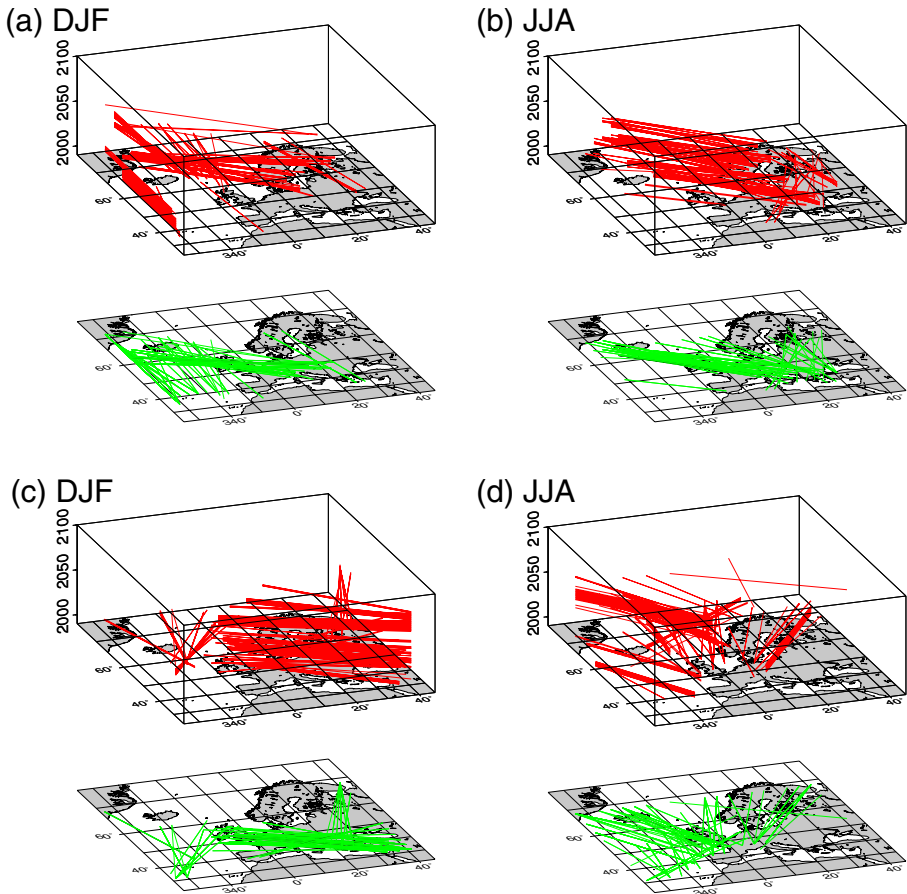
Fig. 7 Same as Figure 5, but for the (a,b) ECHAM5 1% CO_2 and the (c,d) CCSM 1% CO_2

maximum response towards summer temperatures, it also integrates some effects of previous month temperature variability. In contrast to the interannual behaviour the winter precipitation shows enhanced year-to-year variations towards the end of the 19th and the whole 20th century (Figure 8c). In summer, the behaviour is vice versa, with a decrease in variability on these time scales in the 18th through 20th centuries compared with the period before (Figure 8d). Winter uncertainties are rather high prior to 1770 with values of around 190 mm per 3 months (Casty et al. 2005b) and explain at least part of the decreased variability of the reconstructed precipitation sums for the 1500–1850 period. Summer uncertainties are smaller than for winters (80 mm per 3 months) and the decrease of variability towards the 20th century could not be traced back to a weak performance of the reconstruction. However Pfister (1992) states that historical data, used during the pre-1688 period, often emphasize extreme conditions. This may provide a misleading sense of the true seasonal or annual mean climate anomalies.

The filtered time series show that the pre-20th century Alpine winter temperatures were generally colder than those of the 1901–2000 period (Figure 9a). The lowest temperatures
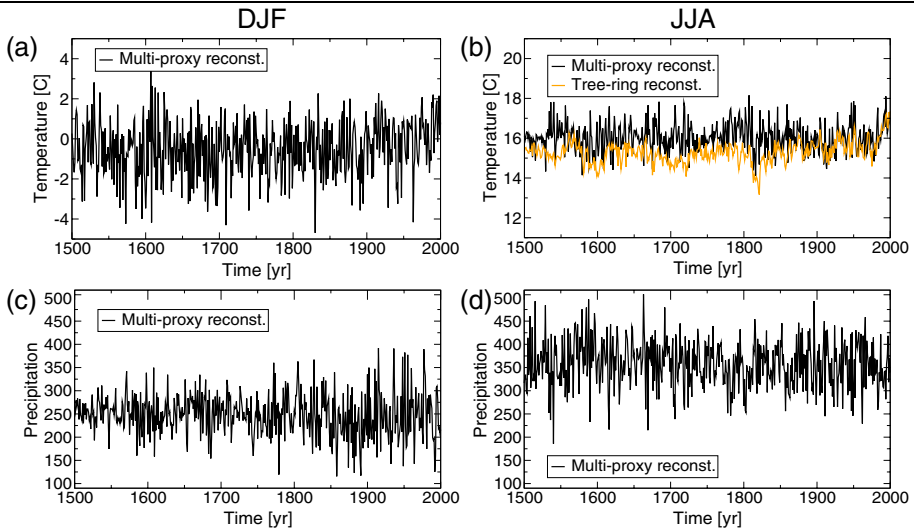
Fig. 8 Unfiltered time series of Alpine temperature and precipitation (unit: mm per 3 months) for (a,c) DJF and (b,d) JJA. The time series are adjusted to the period 1961–1990. The multi-proxy reconstructions (black lines) are based on Casty et al. (2005b) and the tree-ring reconstruction (yellow line) on Büntgen et al. (2005)
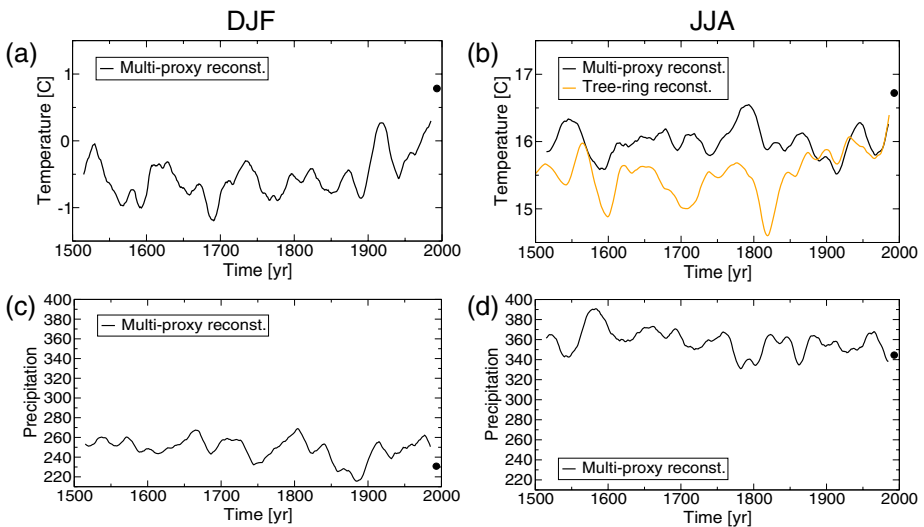

Fig. 9 Filtered time series of Alpine temperature and precipitation (unit: mm per 3 months) for (a,c) DJF and (b,d) JJA. The time series are adjusted to the period 1961–1990. A 31-yr triangular filter is used emphasising the low-frequency variability in the time series. The multi-proxy reconstructions (black lines) are based on Casty et al. (2005b) and the tree-ring reconstruction (yellow line) on Büntgen et al. (2005). To show the tendency of the last decades (which are partly excluded by the filter) the mean from 1986–2000 is denoted by dots for both variables and seasons, respectively

were experienced during the last decades of the 17th century, which is in agreement with the coldest phase over Europe back to 1500 (Luterbacher et al. 2001, 2004). Winters in the 1690s were extremely harsh in the Alpine area with temperature anomalies of the order of −1.2°C compared to 0 °C for the 20th-century mean. Less intense cold periods are reconstructed for the second half of the 16th century and at the end of the 19th century.

A strong transition to a warming in Alpine winters is found from around 1890 to 1915. A cooling is then experienced in the mid-20th century followed by an unprecedented upward trend until recent times (illustrated by dots in Figure 9 that represent the mean of the last 15 years).

In summer the two filtered proxy time series are again analysed and compared. The major difference between the multi-proxy and the tree-ring reconstruction is that the latter shows a clear trend from 1800 to 2000 starting from a lower temperature mean the century before. Again, this amplitude difference could partly be related to the fact that the tree-ring reconstructions also integrates temperature information from before the vegetation period. This extended response period likely reflects lower frequency, inter-decadal scale variability (Figure 9b). Therefore, a better agreement between the two reconstructions could be achieved by comparing the tree-ring reconstruction with the smoothed annual Alpine multi-proxy reconstruction. Moreover, both reconstructions are calibrated against different data. The use of the new homogenised temperatures series of Switzerland (Begert et al. 2005) for both reconstructions data set could also lead to a better agreement. For the multi-proxy reconstruction, warm Alpine summers were experienced around 1550, periodically in the 17th century, the second half of the 18th century, in the mid 20th century, and from 1970 onward (Figure 9b). Except for 1550s, the tree-ring reconstruction resembles this multi-decadal behaviour of the multi-proxy reconstruction, even though the multi-proxy reconstruction and the tree-ring reconstruction are not exactly parallel. For both reconstructions cold summer periods are found at the end of the 16th century, the end of the 17th century, the early 18th century, and the beginning of the 20th century. Summarizing, the discrepancies between the multi-proxy and the tree-ring reconstruction can be traced back to the differing seasonalities represented by the reconstructions, the use of different (predictand) instrumental data, and finally, differing calibration methods during different calibration periods (Büntgen et al. 2005).

For both seasons the reconstructed precipitation time series show that strong decadal to interdecadal changes are superimposed on a general downward trend until the end of the 19th century (Figure 9c,d). The driest period in winter is at the turn of the 20th century followed by a strong upward trend within the 20th century. Very wet summers occurred from 1550 to 1600. The recent downward trend of precipitation over the Alps after 1970 is a result of the trend in the NAO to its positive phase in winter. Statistically significant negative correlations of around -0.5 are found during this period (Casty et al. 2005b). During summer the Azores High gets more pronounced, contributing to the downward trend in precipitation over the Alps (Dünkeloh and Jacobeit 2003; Xoplaki et al. 2004).

To get an idea of the future behaviour of the Alps under global climate change, time slice simulations with a regional model are carried out. In the A2 simulation (2071 to 2100) the winter and summer temperatures show an average rise of about $3°C$ and $4°C$, respectively (Figure 10a,b). Comparing the control time slice 1961–1990 with the A2 scenario, the interannual variability is unchanged in winter, whereas a strong increase on these time scales in summer is observed (Schär et al. 2004). Precipitation behaves differently; in winter a small average increase is simulated in the A2 scenario (Figure 10c). The simulated trend in winter precipitation for the control period 1961–1990 is consistent with the observed trend (Schmidli et al. 2002) and the reconstruction (Figure 9c); thus it may be explained by internal variability. In summer the mean precipitation shows a small decrease compared with the mean of the control simulation (Figure 10d). The interannual variability of precipitation remains unchanged in winter, but increases in summer, comparing the A2 with the control simulation.
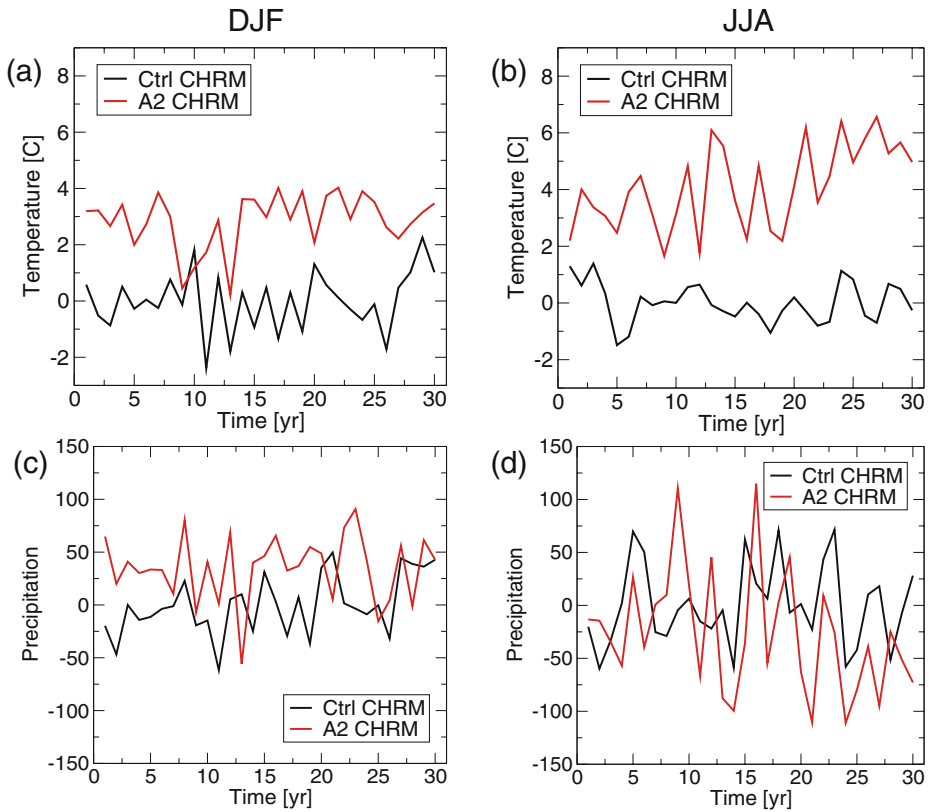
DJF   JJA

Fig. 10 Temperature (a,b) and precipitation (c,d) anomalies of regional simulations for the control time-slice 1961-1990 and the A2 scenario from 2071–2100: (a,c) DJF, (b,d) JJA. Anomalies are taken with respect to the mean of the control simulation 1961-1990. The unit of precipitation is mm per 3 months

5 Summary and conclusions

To improve the understanding of natural climate variability and to assess future climate change, both reconstructions and model simulations are analysed for the Atlantic-European and the Alpine regions.

The time series for temperature and precipitation show variations on interannual to decadal time scales. The recent upward temperature trend for Atlantic-European region is unprecedented over the last 500 years for winter and summer, resembling findings from Jones and Mann (2004) for the Northern Hemisphere and will continue for the next 100 years under the constraint that greenhouse gas emissions will rise (simulated by two coupled GCMs with a 1% CO_2 increase per year). The precipitation signal is not as clear, as the future simulations do not agree in tendency. Going back in time, distinct cold periods are found in the reconstructions, which are separated from the coupled GCM simulation forced with constant 1990 conditions (CCSM 1990). This is mainly due to the difference in radiative forcing over the last 500 years, which was lower at certain stages than the 1990 values used in the simulations. The overlaid reconstructed decadal variability, however, is not distinguishable from the CCSM 1990, leading to a signal detection problem as mentioned by Yoshimori et al. (2005). Recently, von Storch et al. (2004) mentioned that regression methods used in

Northern Hemisphere reconstructions of this kind underestimate low-frequency variability, which leads to the conclusion that the real climate variability shows stronger decadal fluctuations and therefore it might be distinguishable from CCSM 1990. However, recent work (Mann et al. 2005; Goosse et al. 2005) suggests that the results of von Storch et al. (2004) may be overstated, implying that the decadal fluctuations reconstructed may be relatively accurate. In this case the signal detection problem would remain. The changes in seasonality show that the reconstructions have a broader range than the model simulations, resembling the results of Jones et al. (2003). A clear signal in the future could not be detected; as the two simulations again do not agree.

Illustrated by the teleconnectivity we showed that low-frequency changes of large-scale atmospheric circulation flow control at least part of the temperature and precipitation variability, e.g., the meridional circulation in the late Maunder Minimum connected with an anomalously cold period and more zonal flow regime with warm temperatures in the 20th century. Temporally, differences between the reconstructed and the simulated teleconnectivity using CCSM 1990 are likely to be due to the constant external forcing of CCSM 1990. Because the scenario simulations show temporally stable axes of teleconnection patterns over several decades, similar to the reconstructions, we hypothesise that time-dependent external forcing (solar, volcanic and greenhouse gases) might support a temporal stabilisation of the patterns. Future investigations of an ensemble of transient model simulations from 1500 onwards will help to address this question in more detail. It will also give us the possibility to test the reconstruction method in order to exclude exclude those, which are the source of stabilization.

Analysing the low-frequency behaviour of temperature and precipitation, the Alpine area shows stronger amplitudes than the Atlantic-European region in summer and winter. However, this result likely derives from the smaller area considered and does not necessarily imply that mountainous regions are more sensitive to large-scale variability and climate change. Projections for the future climate with a regional model show, beside a clear temperature increase in both seasons, a change in interannual variability in summer. Temperature and precipitation show broader distributions, which could be partly explained by a soil moisture precipitation feedback mechanism (Schär et al. 1999, 2004). However, the reconstructions show an opposite behaviour, comparing the period after 1900 (which is already influenced by increasing greenhouse gas emissions) with the centuries before. Still, it can not be decided whether or not this is due to the underestimation of variability of regression techniques used for the reconstructions, or the regional model's overestimation of the variability, or the past warming was small compared with the expected future warming. A further improvement of the reconstruction methods as well as multi-model ensemble approaches (using different regional models nested in different global models) could give a more comprehensive picture in future.

References

Appenzeller C, Stocker TF, Anklin M (1998) North Atlantic Oscillation dynamics recorded in Greenland ice cores. Science 282:446–449

Arakawa A, Lamb VR (1981) A potential enstrophy and energy conserving scheme for the shallow water equations. Mon Wea Rev 109:18–36

Bauer E, Claussen M, Brovkin V, Huenerbein A (2003) Assessing climate forcings of the Earth system for the past millennium. Geophys Res Lett 30, DOI:10.1029/2002GL016639

Begert M, Schlegel T, Kirchhofer W (2005) Homoteneous temperature and precipitation series of Switzerland from 1864 to 2000. Int J Climatol 25:65–80

Blackmon ML, Boville B, Bryan F, Dickinson R, Gent Kiehl J, Moritz R, Randall D, Shukla J, Solomon S, Bonan G, Doney S, Fung I, Hack J, Hunke E, Hurrell J, Kutzbach J, Meehl J, Otto-Bliesner B, Saravanan R, Schneider EK, Sloan L, Spall M, Taylor K, Tribbia J, Washington W (2001) The community climate system model. Bull Am Meteorol Soc 82:2357–2388

Böhm R, Auer I, Brunetti M, Maugeri M, Nanni T, Schöner W (2001) Regional temperature variability in the European Alps: 1760–1998 from homogenized instrumental series. Int J Climatol 21:1779–1801

Bradley R, Jones PD (1993) Little Ice Age" summer temperature variations: Their nature and relevance to recent global warming trends. The Holocene 3:367–376

Briffa KR, Jones PD, Bartholin TS, Eckstein D, Schweingruber FH, Karlen W, Zetterberg P, Eronen M (1992) Fennoscandian summers from AD 500: Temperature changes on short and long timescales. Clim Dyn 7:111–119

Briffa KR, Osborn TJ, Schweingruber FH, Harris IC, Jones PD, Shiyatov SG, Vaganov EA (2001) Low-frequency temperature variations from a northern tree-ring density network. J Geophys Res 106:2929–2941

Büntgen U, Esper J, Frank DC, Nicolussi K, Schmidhalter M (2005) A 1052-year tree-ring proxy for Alpine summer temperatures. Clim Dyn 25:141–153

Casty C, Handorf D, Raible CC, Luterbacher J, Weisheimer A, Xoplaki E, Gonzalez-Rouco JF, Dethloff K, Wanner H (2005a) Recurrent climate winter regimes in reconstructed and modelled 500 hPa geopotential height fields over the North Atlantic-European sector 1659–1990. Clim Dyn 24:809–822, DOI:10.1007/s00382-004-0496-8

Casty C, Wanner H, Luterbacher J, Esper J, Böhm R (2005b) Temperature und precipitation variability in the European Alps since 1500. Int J Climatol 25:1855–1880

Cheng W, Beck R, Rooth C (2004) Multi-decadal thermohaline variability in an ocean-atmosphere general circulation model. Clim Dyn 22:573–590, DOI:10.1007/s00382-004-400-6

Cook ER, D'Arrigo RD, Mann ME (2002) A well-verified, multiproxy reconstruction of the winter North Atlantic Oscillation index since AD 1400. J Climate 15:1754–1764

Cook ER, Esper J, D'Arrigo RD (2004) Extra-tropical Northern Hemisphere land temperature variability over the past 1000 years. Quat Sci Rev 23:2063–2074

Crowley TJ (2000) Causes of climate change over the past 1000 years. Science 289:270–277

Dünkeloh A, Jacobeit J (2003) Circulation dynamics of Mediterranean precipitation variability 1948–98. Int J Climatol 23:1843–1866

Esper J (2000) Long term tree-ring variations in Junipers at the upper timberline in the Karakorum (Pakistan). The Holocene 10:253–260

Esper J, Cook ER, Schweingruber FH (2002a) Low-frequency signals in long tree-line chronologies for reconstructing past temperature variability. Science 295:2250–2253

Esper J, Frank DC, Wilson RJS (2004) Climate reconstructions: Low-frequency ambition and high-frequency ratification. EOS, Trans Am Geophys Union 85:113,120

Esper J, Schweingruber FH, Winiger M (2002b) 1300 years of climate history for Western Central Asia inferred from tree-rings. The Holocene 12:267–277

Esper J, Shiyatov SG, Mazepa VS, Wilson RJS, Graybill DA, Funkhouser G (2003) Temperature-sensitive Tien Shan tree ring chronologies show multi-centennial growth trends. Clim Dyn 21:699–706

Frank DC, Esper J (2005) Temperature reconstructions and comparison with instrumental data from a tree-ring network for the European Alps. Int J Climatol 25:1437–1454

Frei C, Christensen JH, Deque M, Jacob D, Jones RG, Vidale PL (2003) Daily precipitation statistics in regional climate models: Evaluation and intercomparison for the European Alps. J Geophys Res 108(D3), 4124, DOI: 10.1029/2002JD002287

Gibson JK, Kallberg P, Uppala S, Hernandez A, Nomura A, Serrano A (1999) ERA description, Version 2 Technical report, ERA-15 Project Report Series, No. 1, ECMWF, Reading, UK. p. 74

Goosse H, Crwoley TJ, Zorita E, Ammann H, Renssen CM, Driesschaert E (2005) Modelling the climate of the last millennium: What causes the differences between simulations. Geophys Res Lett 32, L06710, DOI:10.1029/2005GL022368

Grötzner A, Latif M, Barnett TP (1998) A decadal cycle in the North Atlantic ocean as simulated by the ECHO coupled GCM. J Climate 11:831–847

Guiot J, Nicault A, Rathgeber C, Edouard J, Guibal F, Pichard G, Till C (2005) Last-millennium summer-temperature variations in western Europe based on proxy data. Holocene 15:489–500

Hagemann S, Duemenil-Gates, L (2001) Validation of the hydrological cycle of ECMWF and NCEP reanalyses using the MPI hydrological discharge model. J Geophys Res 106:1503–1510

Hansen J, Lacis A, Ruedy R, Sato M (1992) Potential climate impact of Mount Pinatubo eruption. Geophys Res Lett 19:215–218

Hurrell, JW (1995) Decadal trends in the North Atlantic Oscillation: Regional temperatures and precipitation. Science 269:676–679

Hurrell JW, Kushnir Y, Ottersen G, Visbeck M (2003) *The North Atlanitc Oscillation: Climate Significance and Environmental Impact*, Vol. 134. Geophysical Monograph Series. p. 279

Hurrell JW, Loon HV (1997) Decadal variations in climate associated with the North Atlantic Oscillation. Clim Change 36:301–326

IPCC (2001) *Climate Change 2001: The Scientific Basis*. Cambridge, UK and New York, NY, USA: Cambridge University Press. Contribution of Working Group I to the Third Assessment Report of the Intergovenmental Panel on Climate Change, p. 881

Jacobeit J, Wanner H, Luterbacher J, Beck C, Philipp A, Sturm K (2003) Atmospheric circulation variability in the North-Atlantic-European area since the mid-seventeenth century. Clim Dyn 20:341–352

Jones PD, Briffa KR, Barnett TP, Tett SFB (1998) High-resolution palaeoclimatic records for the last millennium: Interpretation, integration and comparison with General Circulation Model control-run temperatures. The Holocene 8:455–471

Jones PD, Briffa KR, Osborn TJ (2003) Changes in the Northern Hemisphere annual cycle: Implications for paleoclimatology. J Geophys Res 108, DOI:10.1029/2003JD003695

Jones PD, Mann ME (2004) Climate over past millennia. Rev Geophys 42, RG2002, DOI:10.1029/2003RG000143

Jones RG, Murphy JM, Hassell DC, Taylor R (2001) Ensemble mean changes in a simulation of the European climate of 2071–2100 using the new Hadley Centre Regional modelling system HadAM3H/HadRM3H, Technical report, Hadley Centre, Exeter, UK, available at http://prudence.dmi.dkl

Kalnay E, Kanamitsu M, Kistler R, Collins W, Coauthors (1996) The NCEP/NCAR 40 year reanalysis project. Bull Am Meteor Soc 77:437–471

Kiehl JT, Hack JJ, Bonan GB, Boville BA, Williamson DL, Rasch PJ (1998) The National Center for Atmospheric Research Community Climate Model: CCM3. J Clim 11:1131–1149

Kistler R, Kalnay E, Collins W, Saha S, Coauthors (2001) The NCEP-NCAR 50-year reanalysis: Monthly means CD-ROM and documentation. Bull Am Meteor Soc 77:437–471

Latif M, Roeckner E, Botzet M, Esch M, Haak H, Hagemann S, Jungclaus J, Legutke S, Marsland S, Mikolajewicz U (2004) Reconstructing, monitoring, and predicting multidecadal-scale changes in the North Atlantic Thermohaline Circulation with sea surface temperature. J Clim 17:1606–1614

Luterbacher J, Dietrich D, Xoplaki E, Grosjean M, Wanner H (2004) European seasonal and annual temperature variability, trends, and extremes since 1500. Science 303:1499–1503

Luterbacher J, Rickli R, Xoplaki E, Tinguely C, Beck C, Pfister C, Wanner H (2001) The late Maunder Minimum (1675–1715) – a key period for studying decadal scale climatic change in Europe. Clim Change 49:441–462

Luterbacher J, Schmutz C, Gyalistras D, Xoplaki E, Wanner H (1999) Reconstruction of monthly NAO and EU indices back to AD 1675. Geophys Res Lett 26:2745–2748

Luterbacher J, Xoplaki E, Dietrich D, Jones PD, Davies TD, Portis D, Gonzalez-Rouco JF, von Storch H, Gyalistras D, Casty C, Wanner H (2002a) Extending North Atlantic Oscillation reconstructions back to 1500. Atmos Sci Lett 2:114–124

Luterbacher J, Xoplaki E, Dietrich D, Rickli R, Jacobeit J, Beck C, Gyalistras D, Schmutz C, Wanner H (2002b) Reconstruction of sea level pressure fields over the Eastern North Atlantic and Europe back to 1500. Clim Dyn 18:545–561

Mann ME, Bradley RS, Hughes MK (1998) Global-scale temperature patterns and climate forcing over the past six centuries. Nature 392:779–787

Mann ME, Rutherford S, Wahl ER, Ammann CM (2005) Testing the fidelity of methodologies used in proxy-based reconstructions of past climate. J Clim 18:4097–4107

Marshall J, Johnson H, Goodman J (2001) A study of the interaction of the North Atlantic Oscillation with ocean circulation. J Clim 14:1399–1421

Marsland SJ, Haak H, Jungclaus JH, Latif M, Roeske F (2003) The Max-Planck-Institute global ocean/sea ice model with orthogonal curvilinear coordinates. Ocean Model 5:91–127

Meehl GA, Washington WM, Wigley TML, Arblaster JM, Dai A (2003) Solar and greenhouse gas forcing and climate response in the twentieth century. J Clim 16:426–444

Mitchell TD, Carter TR, Jones PD, Hulme M, New, M (2004) A comprehensive set of high-resolution grids of monthly climate for Europe and the globe: The observed record (1901–2000) and 16 scenarios (2001–2100). Technical Report Working Paper 55, Tyndall Center for Climate Change Research

Moberg A, Sonechkin DM, Holmgren K, Datsenko NW, Karlen W (2005) Highly variable Northern Hemisphere temperatures reconstructed from low- and high-resolution proxy data. Nature 433:613–617

New M, Hulme M, Jones PD (2000) Representing twentieth-century space-time climate variability. Part II: Development of 1901–1996 monthly grids of terrestrial surface climate. J Clim 13:2217–2238

Overpeck J, Hughen K, Hardy D, Bradley R, Case R, Douglas M, Finney, B, Gajewski K, Jacoby G, Jennings A, Lamoureux S, Lasca A, MacDonald G, Moore J, Retelle M, Smith S, Wolfe A, Zielinski G (1997) Arctic environmental change of the last four centuries. Science 278:1251–1256

Pauling A, Luterbacher J, Casty C, Wanner H (2006) 500 years of gridded high-resolution precipitation reconstructions over Europe and the connection to large-scale circulation. Clim Dyn 26:387–405

Pfister C (1992) Monthly temperature and precipitation in Central Europe 1525–1979: Quantifying documentary evidence on weather and its effects. In: Bradley RS, Jones PD (eds) Climate since A.D. 1500. Routledge, London

Pope DV, Gallani M, Rowntree R, Stratton A (2000) The Impact of new physical parameterizations in the Hadley Centre climate model HadAM3. Clim Dyn 16:123–146

Raible CC, Luksch U, Fraedrich K (2004) Precipitation and Northern Hemisphere Regimes. Atmos Sci Lett 5:43–55, DOI:10.1016/j.atmoscilet.2003.12.001

Raible CC, Luksch U, Fraedrich K, Voss R (2001) North Atlantic decadal regimes in a coupled GCM simulation. Clim Dyn 18:321–330

Raible CC, Stocker TF, Yoshimori M, Renold M, Beyerle U, Casty C, Luterbacher J (2005) Northern Hemispheric trends of pressure indices and atmospheric circulation patterns in observations, reconstructions, and coupled GCM simulations. J Clim 18:3968–3982

Renold M, Beyerle U, Raible CC, Knutti R, Stocker TF, Craig T (2004) Climate modeling with a Linux cluster, EOS, Trans Am Geophys Union 85:292

Rind D, Lean J, Healy R (1999) Simulated time-dependent climate response to solar radiative forcing since 1600. J Geophys Res 104:1973–1990

Roeckner E, Bäuml G, Bonaventura L, Brokopf R, Esch M, Giorgetta M, Hagemann S, Kirchner I, Kornblueh L, Manzini E, Rhodin A, Schlese U, Schulzweida U, Tompkins A (2003) The atmospheric general circulation model ECHAM5: Part I: Model description, Technical Report 349, Max-Planck-Institut, Hamburg, Germany

Schär C, Lüthi D, Beyerle U, Heise E (1999) The soil-precipitation feedback: A process study with a regional climate model. J Clim 12:722–741

Schär C, Vidale PL, Lüthi, D, Häberli C, Liniger MA, Appenzeller C (2004) The role of increasing temperature variability in European summer heatwaves. Nature 427:332–336

Schmidli J, Schmutz C, Frei C, Wanner H, Schär C (2002) Mesoscale precipitation variability in the Alpine region during the 20th century. Int J Climatol 22:1049–1074

Shindell DT, Schmidt GA, Miller RL, Mann ME (2003) Volcanic and solar forcing of climate change during the preindustrial era. J Clim 16:4094–4107

Shindell DT, Schmidt GA, Miller RL, Rind D (2001) Northern Hemisphere winter climate response to greenhouse gas, ozone, solar, and volcanic forcing. J Geophy Res 106:7193–7210

Terray L, Valcke S, Piacentini A (1998) The OASIS coupler user guide, version 2.2, Technical Report TR/CMGC/98–05, CERFACS

Ulbrich U, Christoph M (1999) A shift of the NAO and increasing storm track activity over Europe due to anthropogenic Greenhouse gas forcing, Clim Dyn 15:551–559

Vidale PL, Lüthi D, Frei C, Seneviratne SI, Schär C (2003) Predictability and uncertainty in a regional climate model. J Geophys Res 108, DOI:10.1029/2002JD002810

Vinther BM, Johnsen SJ, Andersen KK, Clausen HB, Hansen AW (2003) NAO signal recorded in the stable isotopes of Greenland ice cores. Geophys Res Lett 30(7), 1387, DOI: 10.1029/2002GL016193

von Storch H, Zorita E, Jones J, Dimitriev Y, Gonzalez-Rouco F, Tett S (2004) Reconstructing past climate from noisy data. Science 306:679–682, DOI:10.1126/science.1096109

Wallace JM, Gutzler DS (1981) Teleconnections in the geopotential height field during the Northern Hemisphere winter. Mon Wea Rev 109:782–812

Wanner H, Brönnimann S, Casty C, Gyalistras D, Luterbacher J, Schmutz C, Stephenson DB, Xoplaki E (2001) North Atlantic Oscillation—concepts and studies. Survey Geophys 22:321–382

Wild M, Calanca P, Scherrer SC, Ohmura A (2003) Effects of polar ice sheets on global sea level in high-resolution greenhouse scenarios, J Geophys Res 108, DOI:10.1029/2002JD002451

Wolff JO, Maier-Reimer E, Legutke S (1997) The Hamburg Ocean primitive equation model HOPE. Technical Report 13, Deutsches Klimarechenzentrum, Hamburg, Germany

Xoplaki E, Gonzalez-Rouco JF, Luterbacher J, Wanner H (2004) Wet season Mediterranean precipitation variability: Influence of large-scale dynamics and trends. Clim Dyn 23:63–78

Xoplaki E, Luterbacher J, Paeth H, Dietrich D, Steiner N, Grosjean M, Wanner H (2005) European spring
    and autumn temperature variability and change of extremes over the last half millennium. Geophys Res
    Lett 32, L15713, DOI: 10.1029/2005GL023424
Yoshimori M, Stocker TF, Raible CC, Renold M (2005) Internal and externally-forced varibilities in an
    ensemble of climate simulations of the Maunder Minimum. J Clim 18:4253–4270